AIAA JOURNAL
Vol. 30, No. 8, August 1992

Multiple Shock-Shock Interference on a Cylindrical Leading Edge

Allan R. Wieting*
NASA Langley Research Center, Hampton, Virginia 23665

This Mach 8 study provides the first detailed pressure and heat transfer rate distributions from a two-dimensional shock wave interference pattern created by two incident oblique shock waves intersecting the bow shock wave of a cylinder. The cylinder is representative of the cowl leading edge of a rectangular hypersonic engine inlet. The peak heat transfer rate was 38 times the undisturbed-flow stagnation-point level and occurred when the two oblique shock waves coalesced before intersecting the cylinder bow shock wave. A new shock-shock interference pattern consisting of concomitant supersonic jets separated from each other by a shear layer and submerged in the subsonic region between the bow shock wave and body has been identified.

Nomenclature

h	= enthalpy
L	= distance between first and second wedge leading edges
M	= Mach number
po	= stagnation pressure behind normal shock wave
pp	= peak pressure
qcw	= heat transfer rate to a wall at a temperature of 290 K (530°R)
qo	= stagnation point heat transfer rate
Re	= unit Reynolds number
T	= temperature
U	= velocity
Δx, Δy	= position of cylinder
δ	= shock generator angle
θ	= angular position on cylinder, positive above undisturbed flow stagnation point, or shock wave angle
ρ	= density
1, 2	= wedge designator

Subscripts

t	= total condition
∞	= freestream

Introduction

SHOCK wave interference heating[1-4] is a critical problem in the structural design of the thermal protection system and the load carrying structure of high-speed vehicles such as the National Aero-Space Plane (NASP). Extremely high pressure and heat transfer rate gradients can occur in highly localized regions where the interference pattern impinges on the surface. The extreme heat transfer rate gradient that occurs over these narrow impingement regions results in a large temperature gradient and attendant thermal stresses,[5] which limit the useful life of the structural component. Experiments before 1987 on these phenomena focused primarily on planar shocks intersecting shock systems generated by three-dimensional bodies or cylinders oriented transverse to the oblique shock (i.e., representative of a wing or tail).[1-4] This left a void for the designer of two-dimensional engine inlets that have planar shocks from the inlet compression surfaces intersecting a cylindrical leading edge oriented with its axis parallel to the plane of the shock. In 1987, Wieting and Holden[6] initiated a unified set of experiments for a cylindrical leading edge oriented with its axis parallel to the plane of the impinging shock. These experiments provided data for the design of cowl leading edges for rectangular hypersonic engine inlets. This study provided the first detailed experimentally pressure and heat transfer rates on a cylindrical leading edge typical of a hypersonic inlet cowl. This initial research was extended in 1988 by Holden et al.[7] to include Mach numbers up to 19 and the effects of leading-edge sweep.[8]

Several investigators have attempted analytical solutions of the shock flowfield. Edney[4] and Morris and Keyes[9] used oblique shock and Prandtl-Meyer expansion relationships to predict the interference pattern and peak pressure and heat transfer rate, with good success. This approach was extended to equilibrium air conditions by Glass.[10] However, these methods rely on experimental measurements of the shock standoff

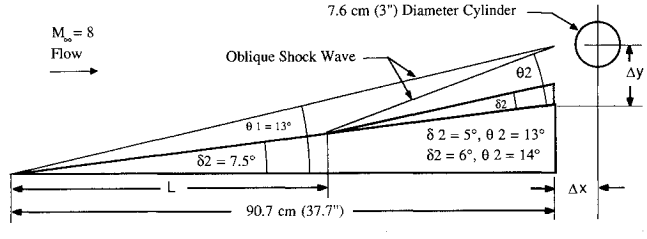

Fig. 1 Schematic of double wedge shock generator and cylinder.

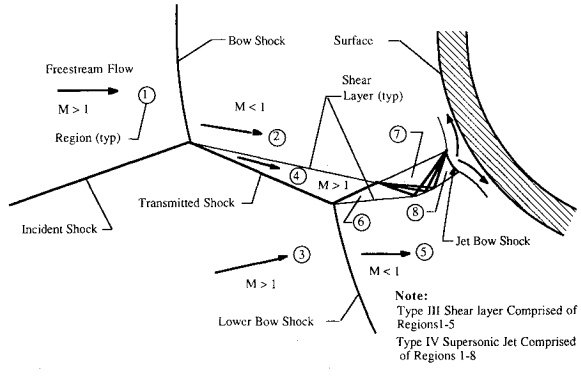

Fig. 2 Schematic of type IV supersonic jet interference pattern.

Presented as Paper 91-1800 at the AIAA 22nd Fluid Dynamics, Plasma Dynamics, and Lasers Conference, Honolulu, HI, June 24-26, 1991; received Aug. 15, 1991; revision received Jan. 13, 1992; accepted for publication Jan. 30, 1992.

*Head, Aerothermal Loads Branch, Mail Stop 395. Member AIAA.

Table 1 Test conditions and model configuration

Run	M_∞	p_∞, kPa	ρ_∞, kg/m^3	T_∞, K	U_∞, m/s	Re, 1/m $\times 10^{-6}$	h_t, J/kg $\times 10^{-5}$	p_t, kPa	T_t, K	$\delta 2$, deg	Δy, cm	Δx, cm	L, cm
21	8.03	0.875	0.0250	122	1780	5.12	3.506	9970	1550	0	7.34	5.31	—
82	8.04	0.844	0.0240	123	1790	4.89	3.537	9670	1560	0	9.91	7.82	—
89	8.04	0.833	0.0235	123	1790	4.79	3.549	9540	1570	0	10.46	7.16	—
87	8.04	0.855	0.0244	122	1780	4.97	3.512	9760	1550	5	10.08	7.16	53.47
83	8.03	0.829	0.0231	125	1800	4.69	3.593	9510	1590	5	10.08	7.16	56.13
85	8.04	0.818	0.0230	123	1800	4.69	3.564	9420	1570	5	10.08	7.16	58.67
88	8.05	1.056	0.0235	130	1840	5.61	3.756	12,300	1650	5	10.08	7.16	58.67
93	8.04	0.820	0.0235	122	1780	4.82	3.497	9330	1550	6	10.16	7.16	54.91
92	8.04	0.848	0.0244	121	1770	5.02	3.483	9650	1540	6	10.16	7.16	56.82
90	8.04	0.839	0.0235	124	1800	4.76	3.579	9610	1580	6	10.16	7.16	59.99
91	8.04	0,838	0.0238	122	1790	4.86	3.534	9580	1560	6	10.16	7.16	59.99
86	8.04	0.820	0.0228	125	1800	4.63	3.600	9410	1590	6	10.08	7.16	61.11
94	8.04	0.834	0.0240	121	1770	4.92	3.486	9460	1540	6	10.16	7.16	63.02
95	8.04	0.845	0.0239	123	1790	4.86	3.549	9620	1570	6	10.80	7.16	63.02

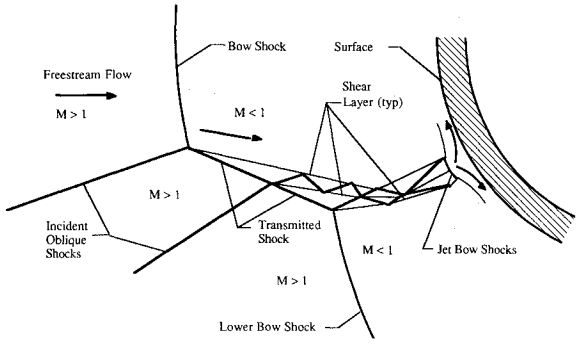

Fig. 3 Schematic of concomitant supersonic jet interference pattern.

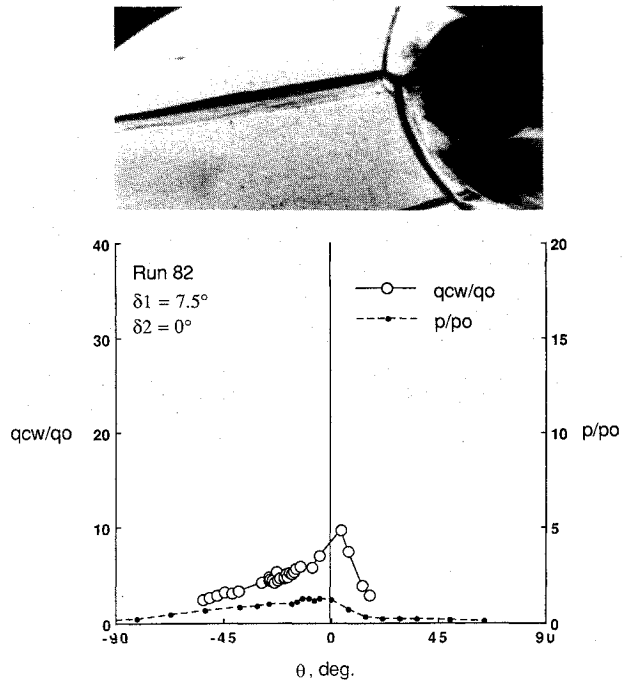

Fig. 4 Schlieren photograph and heat transfer rate and pressure distribution for single incident shock: Δx = 7.82 cm; Δy = 9.91 cm.

distance and transmitted shock length. Two dimensional Navier-Stokes analyses by Thareja et al.[11] using unstructured grids have been very successful. However, the effect of shear-layer turbulence remains unquantified.[12]

This paper presents the first detailed pressure and heat transfer rate distributions on a cylinder resulting from a two-dimensional shock wave interference pattern created by two incident oblique shock waves intersecting the bow shock wave of a cylinder. The experimental results were obtained from tests in the Calspan University of Buffalo Research Center 48-in. Hypersonic Shock Tunnel (48″ HST) at a nominal Mach number of 8. The position of the cylinder and the second wedge was varied to obtain various shock interference patterns.

Test Apparatus

The tests in the 48″ HST were at a nominal Mach number of 8, total temperatures of 1550 K (2800°R), freestream unit Reynolds number of 4.9×10^6/m (1.5×10^6/ft). Single frame schlieren was obtained. Test conditions and model configurations are given in Table 1.

A schematic of the model is shown in Fig. 1. The engine leading edge was simulated with a 1.3-cm-thick, 46-cm-long, 7.6-cm-diam 321 stainless steel cylinder. The large diameter was required to provide the detailed surface distributions of pressure and heat transfer rate. The vehicle compression surfaces were simulated with a sharp leading edge 7.5-deg shock generator wedge, and interchangeable 5- or 6-deg wedges, which were mounted approximately 53 cm L downstream of the leading edge of the first wedge. The 5- or 6-deg wedge could be translated along the surface of the first wedge, and the cylinder could be translated horizontally Δx or vertically Δy to facilitate obtaining the desired shock intersection location or the desired shock-shock interference pattern. In addition, the cylinder could be rotated about its axis to place the high-density instrumentation in the interaction zone. The cylinder was mounted with its axis parallel to the plane of the shock generators. Shock wave angles for the various wedges are given in the figure.

The test time was 15 ms; therefore, high-frequency pressure transducers and thin film platinum resistance thermometers were used. The model had 25 pressure locations and 30 heat transfer locations. The pressure locations were 2.4 deg or 0.0169 cm apart. The heat transfer gauges were mounted on a Pyrex substrate and spaced 0.76 deg or 0.051 cm apart in the high-density area and 3.05 deg or 0.0203 cm elsewhere.

Pressure and thermometer gauge output were converted to engineering units in the normal manner. The temperature histories were converted to heat transfer rates using a numerical procedure based on the solution for a semi-infinite solid with temperature dependent properties.[13] Overall accuracy was within 5%. See Refs. 6–8 for more detail.

Results and Discussion

Shock Wave Interference Patterns

The first step in determining the effect of shock wave impingement on the pressure and heat transfer rate is to determine the interference pattern that will exist when oblique shocks of different strengths intersect. The type of interfer-

ence pattern obtained is dependent on the relative strengths of the intersecting shocks and the geometry of the body on which the extraneous shock system will impinge. Edney[4] defined six types of shock wave interference patterns, all of which can occur when a single oblique shock wave intersects the bow shock wave of a leading edge. The six interference patterns change as the impinging-shock bow-shock intersection point moves circumferentially around the cylinder. Three of the interference patterns (types I, II, and V) result in shock/boundary-layer interactions. A type III results in an attaching shear layer, and a type VI results in an expansion-fan boundary-layer interaction. Type IV is characterized by an impinging or grazing supersonic jet. The details of the interference patterns are described in detail by Edney.[4] Although the interference patterns that occur in this study are created by two incident oblique shock waves, they are essentially type III or IV, which are briefly described in the following.

Type III Interference

A type III interference pattern occurs when a weak oblique shock wave intersects a strong shock wave (flow behind the shock wave is subsonic). The flow in the region above the shear layer is subsonic, and the flow between the shear layer and transmitted shock is supersonic. Depending on the angle the shear layer makes with the tangent to the body surface, the shear layer will be undeflected and attached to the surface.

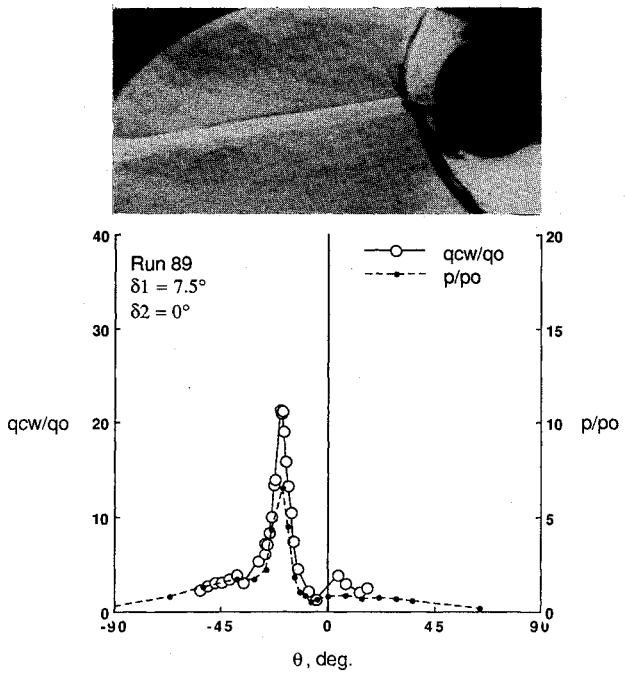

Fig. 5 Schlieren photograph and heat transfer rate and pressure distribution for single incident shock: $\Delta x = 7.16$ cm; $\Delta y = 10.46$ cm.

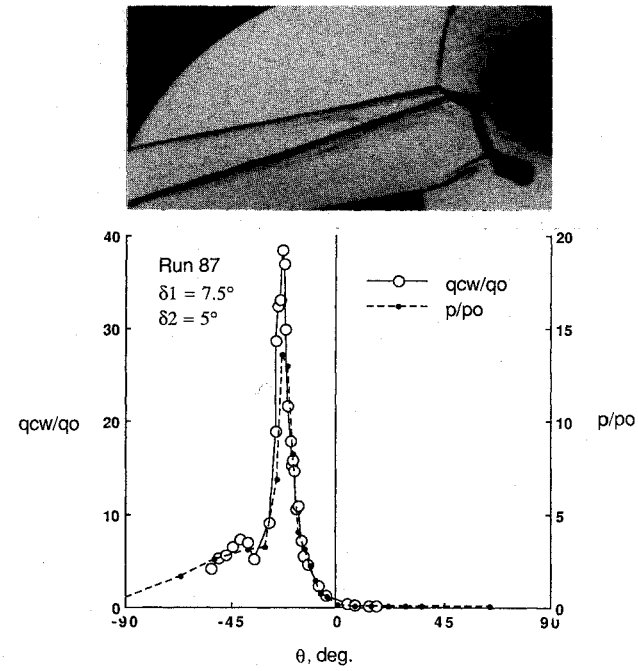

Fig. 7 Schlieren photograph and heat transfer rate and pressure distribution for dual incident shock: $L = 53.47$ cm.

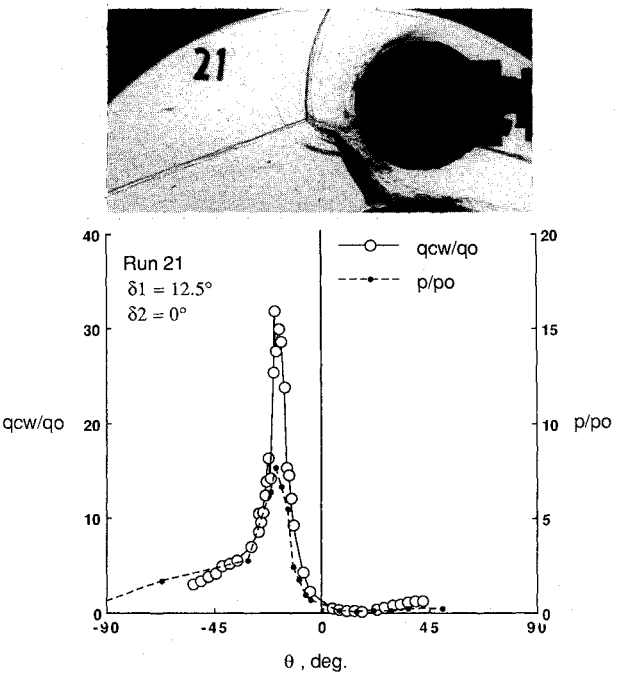

Fig. 6 Schlieren photograph and heat transfer rate and pressure distribution for single incident shock: $\Delta x = 5.31$ cm; $\Delta y = 7.34$ cm.

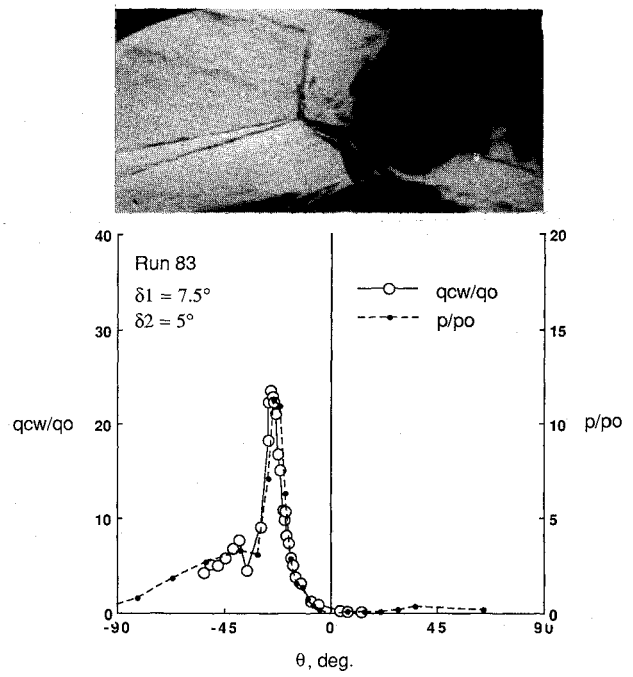

Fig. 8 Schlieren photograph and heat transfer rate and pressure distribution for dual incident shock: $L = 56.13$ cm.

The supersonic flow is deflected downward through an oblique shock, the strength of which is dependent on the Mach number and flow turning angle. Pressure and heat transfer rate amplification caused by the attaching shear layer is analogous to a reattaching separated boundary layer. The heat transfer rate is dependent on the Reynolds number of the impinging flow based on the shear layer length. The state of the shear layer (laminar or turbulent) is a critical parameter in determining the pressure and heat transfer rates.

Type IV Interference

The type IV supersonic jet interference pattern, shown as Fig. 2, occurs when an oblique shock wave intersects the nearly normal part of the bow shock wave from a blunt leading edge. The intersection results in further displacement of the bow shock wave and the formation of a supersonic jet contained between two shear layers and submerged within the subsonic shock layer between the body and the bow shock wave. A jet bow shock is produced when the jet impinges on the surface, creating a small region of stagnation heating. The maximum pressure and heat transfer rates occur when the jet impinges perpendicular to the surface.

The admissible shock-shock interference patterns are best determined by constructing pressure deflection diagrams, as demonstrated by Edney[4] for a single incident shock wave. Pressure deflection diagrams for two incident oblique shock

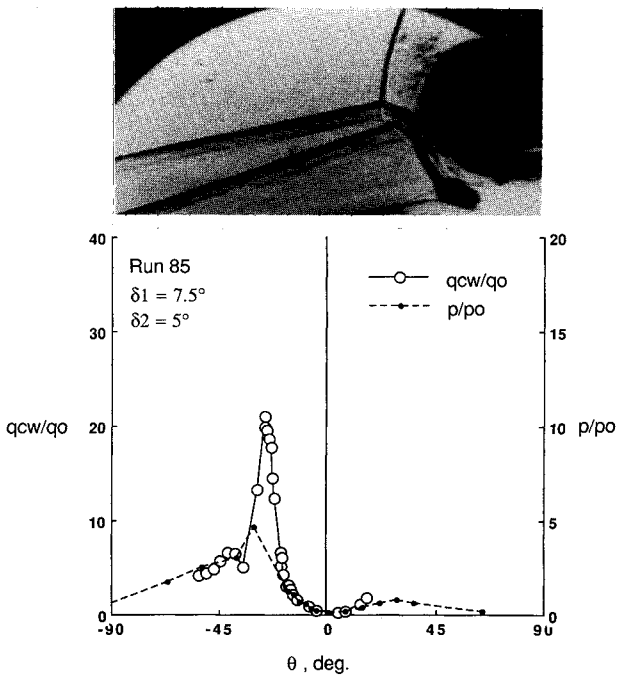

Fig. 9 Schlieren photograph and heat transfer rate and pressure distribution for dual incident shock: L = 58.67 cm.

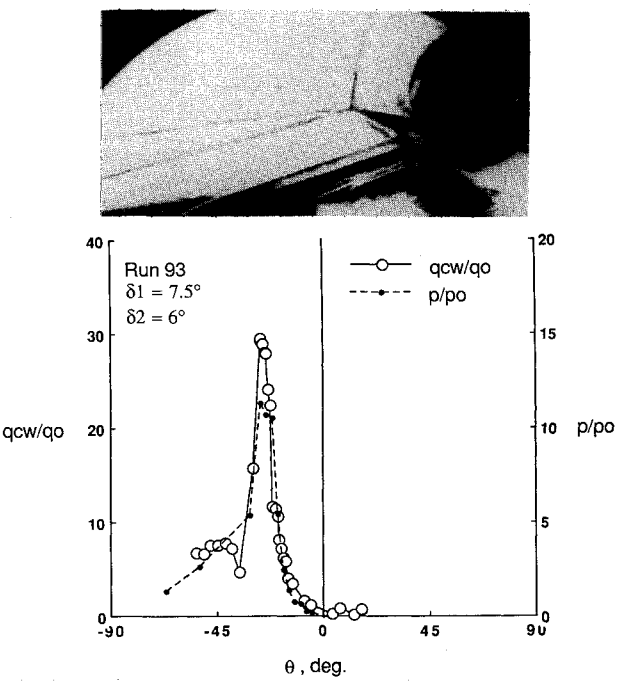

Fig. 11 Schlieren photograph and heat transfer rate and pressure distribution for dual incident shock: L = 54.91 cm.

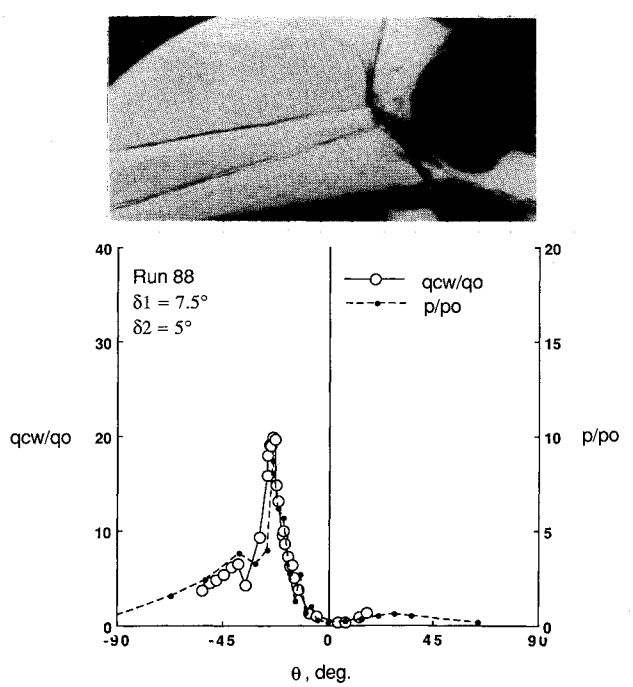

Fig. 10 Schlieren photograph and heat transfer rate and pressure distribution for dual incident shock: L = 58.67 cm.

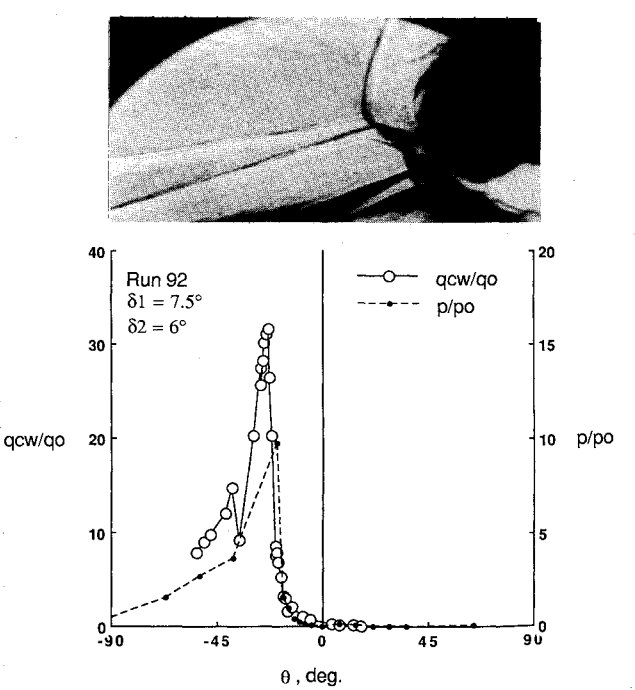

Fig. 12 Schlieren photograph and heat transfer rate and pressure distribution for dual incident shock: L = 56.82 cm.

Table 2 Peak amplification ratios and locations

Run	Heat transfer θ, deg	Heat transfer qp/qo	Pressure θ, deg	Pressure pp/po	$\delta 2$, deg
		Single incident shock			
21	−19.58	31.78	−19.10	7.61	0
82	4.11	4.88	−4.77	2.58	0
89	−19.88	21.28	−19.10	6.55	0
		Dual incident shock			
87	−23.87	38.44	−23.87	13.57	5
83	−25.47	23.43	−23.87	11.24	5
85	−26.27	20.98	−31.04	4.66	5
88	−23.87	19.86	−23.87	8.73	5
93	−26.27	29.43	−26.26	11.30	6
92	−23.07	31.62	−19.10	9.71	6
90	−26.27	24.52	−26.26	9.84	6
91	−26.27	18.91	−23.87	9.19	6
86	−5.06	7.67	−9.55	2.70	6
94	−14.80	8.62	−52.52	2.51	6
95	−46.16	14.33	−45.36	6.18	6

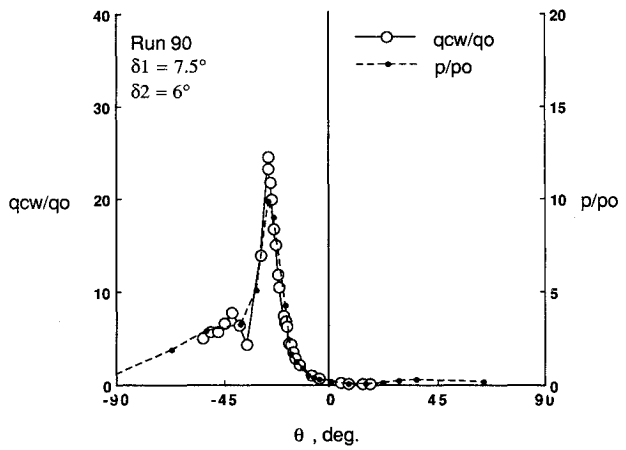

Fig. 13 Heat transfer rate and pressure distribution for dual incident shock: L = 59.99 cm.

waves are presented in Ref. 14 by Wieting for the data presented herein. By generating pressure deflection diagrams, Wieting identified a new interference pattern, shown schematically in Fig. 3, that consists of concomitant supersonic jets separated from each other by a shear layer.

Experimental Results

The undisturbed pressures and heat transfer rates, normalized by the stagnation point values, are plotted in Figs. 4–17 as a function of angular position θ measured in degrees from the horizontal centerline of the cylinder. A schlieren photograph of the interference pattern is also presented. Tabulated data is given in Ref. 14. The peak pressure and heat transfer amplification ratios and their locations are given in Table 2. The amplification ratio is defined as the ratio of the peak pressure or the peak heat transfer rate caused by the impingement of the shock wave interference pattern to the undisturbed freestream stagnation pressure or heat transfer rate.[15]

Single Incident Shock Wave

The pressure and heat transfer rate distributions along the circumference of the cylinder for a type IV supersonic jet interaction are given in Figs. 4–6. The results shown in Figs. 4 and 5 are for the 7.5-deg wedge and in Fig. 6 for a 12.5-deg wedge. As shown in Fig. 4, the supersonic jet is turned upward and grazes the surface at $\theta = 4.11$ deg, resulting in a low heat transfer and pressure amplification. The supersonic jet impinges nearly perpendicular at $\theta \sim -19$ deg in Figs. 5 and 6, resulting in heat transfer rate amplifications of 21 and 32, respectively. The difference in the latter two is due to the different strengths of the impinging oblique shock wave.

Dual Incident Shock Wave

The type of interference pattern obtained is dependent on the strength of the impinging shock waves and their intersection points on the body's bow shock wave. The pressure and heat transfer rate amplifications are dependent on both the interference pattern and the flow angle of incidence with the surface. The cylinder and/or second wedge were moved, as indicated in Table 1, to change the intersection point of the

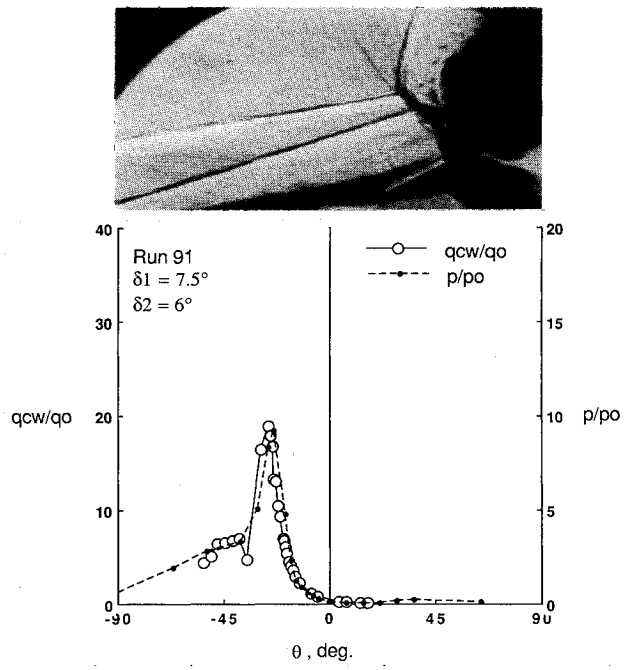

Fig. 14 Schlieren photograph and heat transfer rate and pressure distribution for dual incident shock: L = 59.99 cm.

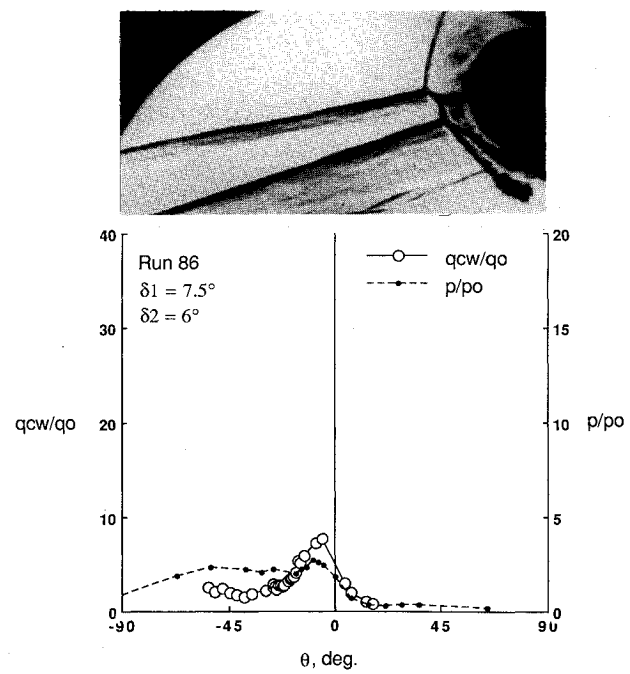

Fig. 15 Schlieren photograph and heat transfer rate and pressure distribution for dual incident shock: L = 61.11 cm.

oblique shock waves. The interference pattern and pressure and heat transfer rate distributions changed as shown in Figs. 7–10 for the 7.5- and 5-deg wedge combination and Figs. 11–17 for the 7.5- and 6-deg wedge combination. In each set, the results start with coalesced incident oblique shock waves and progress through the interference patterns created by the noncoalesced incident shock waves. The schlieren photographs and pressure deflection diagrams[14] indicate that type IV and type III interference patterns occurred with the exception of the concomitant supersonic jet pattern.

The corresponding pressure and heat transfer rate distributions indicate that the peak amplification ratios occur when the two incident oblique shock waves coalesced (Figs. 7 and 11) before intersecting the cylinder bow shock wave. As the

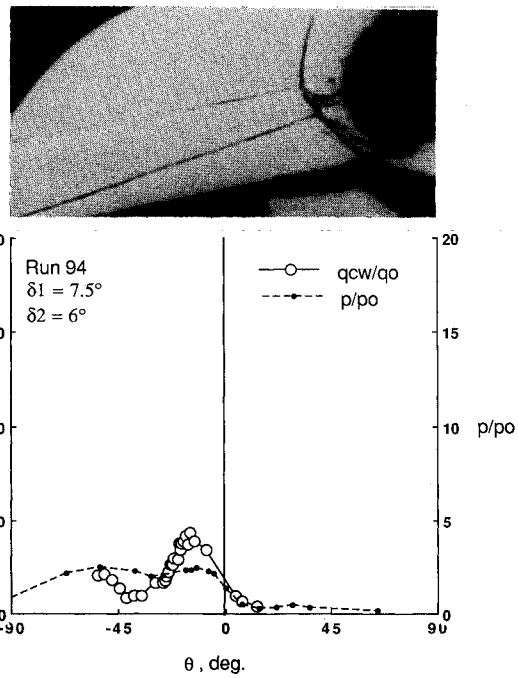

Fig. 16 Schlieren photograph and heat transfer rate and pressure distribution for dual incident shock: L = 63.02 cm.

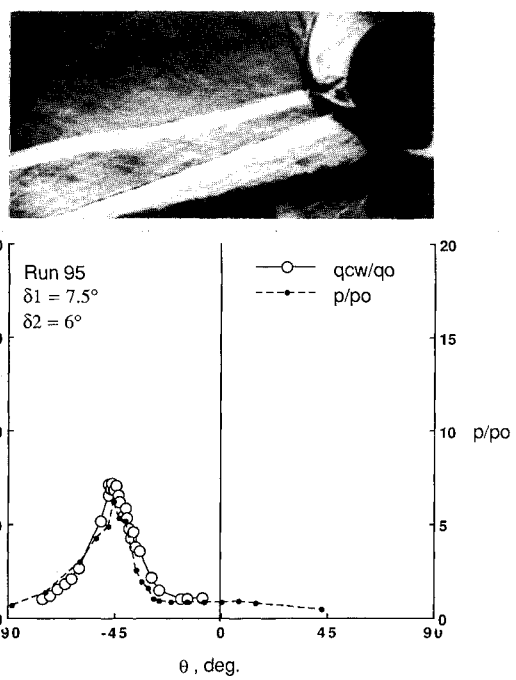

Fig. 17 Schlieren photograph and heat transfer rate and pressure distribution for dual incident shock: L = 63.02 cm.

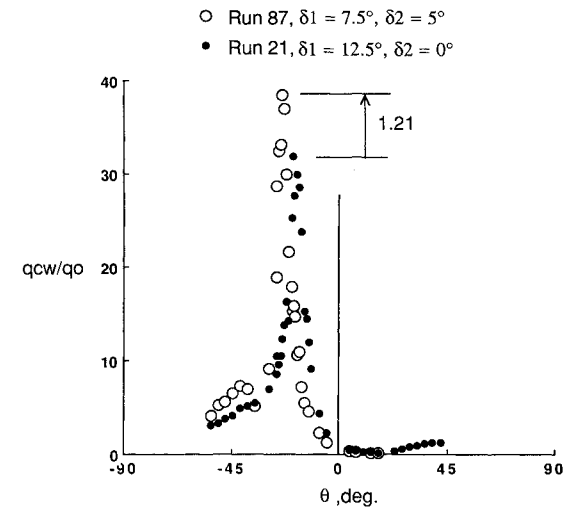

Fig. 18 Comparison of heat transfer rate distribution for flows turned by a single 12.5-deg wedge and one turned by a 7.5- and then a 5-deg wedge.

second wedge was translated downstream, its oblique shock wave intersected the transmitted shock wave (see Fig. 2) created by the first oblique shock wave and a new shock interference pattern occurred. This new concomitant supersonic jet pattern consisted of two supersonic jets separated from each other by a shear layer and they in turn were separated from the subsonic regions by shear layers, as shown in Fig. 3. The schlieren photograph and heat transfer rate and pressure distribution for this pattern are shown in Figs. 8–10 and 12–14. In general, the peak heat transfer rate was less than the level for the coalesced case. When the second oblique shock wave intersected the lower bow shock wave, the interference pattern would either be a dual type IV or type III or a type IV and a type III, as shown in Figs. 15 and 16. In these cases, the peak heat transfer rate occurs where the supersonic jet interacts with the surface, but the peak level is lower than the level for the single oblique shock wave created by the 7.5-deg wedge. In run 95, Fig. 17, the cylinder was moved upward and the peak heat transfer rate occurred at the location where the shear layer impinged instead of where the supersonic shear layer grazed the surface.

A direct comparison of the heat transfer rate distribution for flow turned 12.5 deg through a single wedge and a combination of 7.5- and 5-deg wedges is made in Fig. 18. The coalesced incident shocks increase the heat transfer rate amplification ratio by 21% in this case. The peak heat transfer rates and pressures are lower for weaker oblique shock waves and when the waves do not coalesce. Therefore, the peak heat transfer rate and pressure to a leading edge can be minimized by compressing the flow through several small wedge angles and not allowing the incident oblique shock waves to coalesce.

Concluding Remarks

This paper presents the details of an experimental study of shock wave interference heating on a cylindrical leading edge representative of the cowl of a rectangular hypersonic engine inlet. The study was conducted at a Mach number of 8. Stream Reynolds number was 4.9×10^6/m (1.5×10^6/ft) and stream total temperature was 1550 K (2800°R). The model consisted of a 7.6-cm-diam cylinder and an initial 7.5-deg shock generator wedge and interchangeable second wedges of 5 and 6 deg. The primary goal of this study was to obtain detailed surface pressure and heat transfer rate distributions along the circumference of the cylinder to fill a void in the data base for both design and code validation. Test results are primarily for the type IV supersonic jet interaction since it represents the most severe pressure and heat transfer rate condition. The experi-

ments were performed in the Calspan University of Buffalo Research Center 48-in. Hypersonic Shock Tunnel.

This study has provided the first detailed heat transfer rate and pressure distributions on a cylinder for two-dimensional shock wave interference created by two incident oblique shock waves intersecting the cylinder bow shock wave. The peak heat transfer rate and pressure amplifications measured were 38 and 14, respectively, and occurred when the two incident oblique shock waves coalesced before intersecting the cylinder bow shock wave. Noncoalesced incident shock waves result in interference patterns consisting of two type IV (two supersonic jets) or type IV and type III (a supersonic jet and a shear layer). A new interference pattern, which consisted of two supersonic jets separated by three shear layers, was identified. The peak heat transfer rate and pressure to an engine leading edge is minimized by compressing the flow through several small wedge angles and not allowing the incident oblique shock waves to coalesce.

References

[1]Ryan, B. M., "Summary of the Aerothermodynamic Interference Literature," Naval Weapons Center, TN 4061-160, China Lake, CA, April 1969.

[2]Korkegi, R. H., "Survey of Viscous Interactions Associated with High Mach Number Flight," *AIAA Journal,* Vol. 9, No. 5, 1971, pp. 771–784.

[3]Keyes, J. W., and Hains, F. D., "Analytical and Experimental Studies of Shock Interference Heating in Hypersonic Flow," NASA TN D-71 39, May 1973.

[4]Edney, B., "Anomalous Heat Transfer and Pressure Distributions on Blunt Bodies at Hypersonic Speeds in the Presence of an Impinging Shock," Astronautics Research Inst. of Sweden, FFA Rept. 115, Stockholm, Feb. 1968.

[5]Dechaumphai, P., Thornton, E. A., and Wieting, A. R., "Flow-Thermal Structural Study of Aerodynamically Heated Leading Edges," *Journal of Spacecraft and Rockets,* Vol. 26, No. 4, 1989, pp. 201–209.

[6]Wieting, A. R., and Holden, M. S., "Experimental Study of Shock Wave Interference Heating on a Cylindrical Leading Edge," *AIAA Journal,* Vol. 27, No. 11, 1989, pp. 1557–1565.

[7]Holden, M., Wieting, A. R., Moselle, J., and Glass, C., "Studies of Aerothermal Loads Generated in Regions of Shock-Shock Interaction in Hypersonic Flow," AIAA Paper 88-0477, Jan. 1988.

[8]Glass, C. E., Wieting, A. R., and Holden, M. S., "Effect of Leading Edge Sweep on Shock-Shock Interference Heating at Mach 8," AIAA Paper 89-0271, Jan. 1989.

[9]Morris, D. K., and Keyes, J. W., "Computer Programs for Predicting Supersonic and Hypersonic Interference Flow Fields and Heating," NASA TM X-2725, May 1973.

[10]Glass, C. S., "Computer Program To Solve Two-Dimensional Shock-Wave Interference Problems with an Equilibrium Chemically Reacting Air Model," NASA TM 4187, Aug. 1990.

[11]Thareja, R., Stewart, J., Hassan, O., Morgan, K., and Peraire, J., "A Point-Implicit Unstructured Grid Solver for the Euler and Navier Stokes Equations," AIAA Paper 88-0036, Jan. 1988.

[12]Wieting, A. R., "Shock Interference Heating in Scramjet Engines," AIAA Paper 90-5238, Oct. 1990.

[13]Carslaw, H. S., and Jaeger, J. C., *Conduction of Heat in Solids,* 2nd ed., Clarendon Press, Oxford, England, UK, 1959.

[14]Wieting, A. R., "Multiple Shock-Shock Interference on a Cylindrical Leading Edge," AIAA Paper 91-1800, June 1991.

[15]Fay, J. A., and Riddell, F. R., "Theory of Stagnation Point Heat Transfer in Dissociated Air," *Journal of the Aeronautical Sciences,* Vol. 25, No. 2, 1958, pp. 73–121.